

Low-power Spike-based Wearable Analytics on RRAM Crossbars

Abhiroop Bhattacharjee^{*§}, Jinquan Shi^{*§}, Wei-Chen Chen[°], Xinxin Wang[°] and Priyadarshini Panda[§]

[§]Department of Electrical Engineering, Yale University, USA

[°] Department of Electrical Engineering, Stanford University, USA

Abstract—This work introduces a spike-based wearable analytics system utilizing Spiking Neural Networks (SNNs) deployed on an In-memory Computing engine based on RRAM crossbars, which are known for their compactness and energy-efficiency. Given the hardware constraints and noise characteristics of the underlying RRAM crossbars, we propose online adaptation of pre-trained SNNs in real-time using Direct Feedback Alignment (DFA) against traditional backpropagation (BP). Direct Feedback Alignment (DFA) learning, that allows layer-parallel gradient computations, acts as a fast, energy & area-efficient method for online adaptation of SNNs on RRAM crossbars, unleashing better algorithmic performance against those adapted using BP. Through extensive simulations using our in-house hardware evaluation engine called *DFA_Sim*, we find that DFA achieves upto 64.1% lower energy consumption, 10.1% lower area overhead, and a $2.1\times$ reduction in latency compared to BP, while delivering upto 7.55% higher inference accuracy on human activity recognition (HAR) tasks.

Index Terms—Spiking Neural Networks, In-memory Computing, Direct Feedback Alignment, Online Adaptation

I. INTRODUCTION

The rise of wearable technologies in edge computing has drawn attention to tasks such as diagnostics, smart healthcare, and fitness monitoring, which often involve real-time time-series data processing (Fig. 1(a)) [1]–[3]. Wearable devices typically operate under low power budgets of less than 1W, especially for tasks like human activity recognition (HAR), physiological monitoring, and predictive health diagnostics [4]–[6]. This makes energy-efficiency crucial in edge systems. Traditional deep learning models, while powerful, are energy-intensive due to dense matrix multiplications and frequent memory access, making them unsuitable for low-power wearables [7], [8]. Today, Spiking Neural Networks (SNNs) have emerged as an energy-efficient alternative with their sparse & event-driven binary spike processing, particularly suited for real-time temporal tasks like ECG, EEG, motion tracking, and speech analysis [1], [6], [9], [10].

From a hardware implementation standpoint, In-memory Computing (IMC) with analog crossbar arrays enables compact, energy-efficient dot-product operations with high parallelism [11], [12]. Unlike traditional von-Neumann architectures like GPUs and TPUs, IMC crossbars keep neural network’s weights stationary, reducing data transfer overhead between the memory and the compute units. This is ideal for

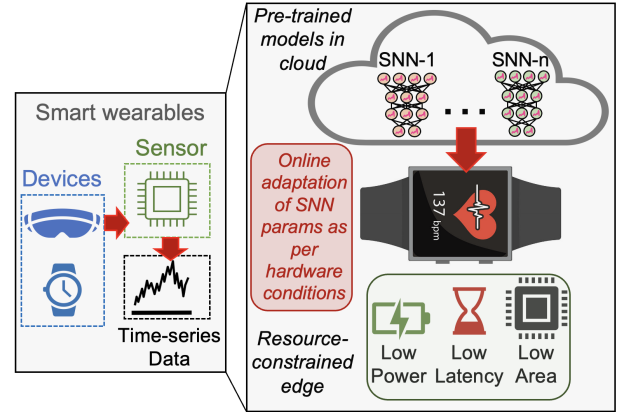


Fig. 1: Pictorial depiction of SNNs used in wearables for temporal data-processing. Pre-trained SNNs in the cloud are adapted online according to the constraints of resource-constrained edge devices.

wearables, which have stringent area and power constraints. IMC-implemented SNNs, with their high spike sparsity and binary computations, offer reduced peripheral circuit and data communication overhead, enhancing energy-efficiency and throughput [13]–[15].

However, IMC-implemented SNNs are prone to non-idealities due to the analog nature of dot-product operations over multiple timesteps [13], [16], [17]. These non-idealities arise from the limited precision and variations in the non-volatile memory (NVM) devices in the crossbars, leading to inaccurate dot-products and reduced inference accuracy [16], [18]. Variation-aware Training (VAT) is widely employed to improve robustness of neural networks against hardware non-idealities [19], [20]. Thus, online adaptation of pre-trained models to the specific hardware conditions & non-idealities is imperative for resource-constrained edge platforms like IMC crossbars (see Fig. 1).

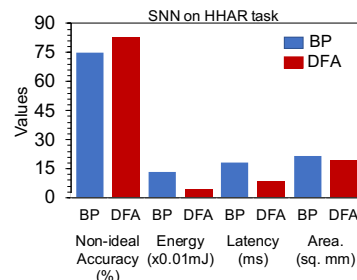


Fig. 2: Plot showing the advantages of DFA-based online SNN adaptation on an IMC platform over traditional BP.

Adapting SNNs on edge devices with minimal energy, latency, and area overhead, while maintaining algorithmic performance, is paramount. However, traditional backpropagation (BP) for online adaptation on IMC platforms faces several challenges: (a) layer-by-layer gradient propagation across multiple timesteps is latency-intensive, and (b) BP requires

* These authors have contributed equally to this work.

This work was supported in part by CoCoSys, a JUMP2.0 center sponsored by DARPA and SRC, the National Science Foundation (CAREER Award, Grant #2312366, Grant #2318152), the DoE MMICC center SEA-CROGS (Award #DE-SC0023198), and the National Science Foundation Expeditions in Computing (Penn State, Award #1317470). The authors acknowledge Weier Wan and Prof. H.-S. Philip Wong for their valuable discussions and insights towards this work.

transposable crossbars, thereby increasing the energy and area costs of peripheral circuits [21], [22]. To address these limitations, we propose a Direct Feedback Alignment (DFA) strategy for online adaptation of pre-trained SNNs on RRAM crossbars, enabling robust inference. Unlike BP, DFA uses localized gradient learning to simultaneously fine-tune all SNN layers on hardware [23]. The key contributions of our work are as follows:

- 1) Development of *DFA_Sim*, our in-house evaluation engine for analyzing the hardware costs of DFA-based online adaptation compared to BP on RRAM crossbars.
- 2) For hardware-realistic SNN accuracy evaluations using *DFA_Sim*, we propose an accurate noise prediction model for RRAM devices in the crossbars using Gaussian Process Regression [24] with experimental data from a real IMC chip called NeuRRAM [25].
- 3) Our experiments show that DFA-based SNN adaptation on a HAR task [26] incurs $2.1\times$ lower latency, 64.1% lower energy, 10.1% lower area, and 7.55% higher inference accuracy on RRAM crossbars compared to BP (see Fig. 2).

II. BACKGROUND

Spiking Neural Networks: As shown in Fig. 3(a), a key characteristic of SNNs is their use of a distinct neuronal activation function, typically the Leaky-Integrate-and-Fire (LIF) model, for temporal signal processing, in contrast to the ReLU activation commonly employed in Artificial Neural Networks (ANNs). The LIF neuron i , with its associated membrane potential u_i^t , integrates a series of spike inputs as follows:

$$u_i^t = \lambda u_i^{t-1} + \sum_j w_{ij} o_j^t. \quad (1)$$

Here, t stands for the timestep, w_{ij} for weight connections between neuron i and neuron j and λ denotes the leak factor. The LIF neuron i generates an output spike o_i^t at the end of timestep t if the membrane potential exceeds a threshold θ :

$$o_i^t = \begin{cases} 1, & \text{if } u_i^t > \theta, \\ 0 & \text{otherwise.} \end{cases} \quad (2)$$

When the neuron fires, its membrane potential resets to zero. The integrate-and-fire mechanism of an LIF neuron leads to a non-differentiable function, which complicates the use of backpropagation for training SNNs. To overcome this challenge, techniques such as Surrogate Gradient Learning or Backpropagation Through Time (BPTT) approximate the backward gradient function [27], enabling direct learning from spikes with fewer timesteps. Additionally, BPTT-based training of SNNs can be implemented using widely-used machine learning frameworks like PyTorch [28].

Moreover, in line with prior work [29], we use direct encoding to convert the input tensor into spike trains across a total of T timesteps. For the final prediction, we run the inference over T timesteps ($t = 1, 2, \dots, T$) and compute the average of the outputs from the SNN classifier.

Analog IMC Crossbars: Analog crossbars comprise of a 2D array of NVM devices, interfaced with Digital-to-Analog Converters (DACs), Analog-to-Digital Converters (ADCs), and write circuits dedicated towards programming the NVM devices [11], [12]. The SNN's spike inputs are encoded as analog

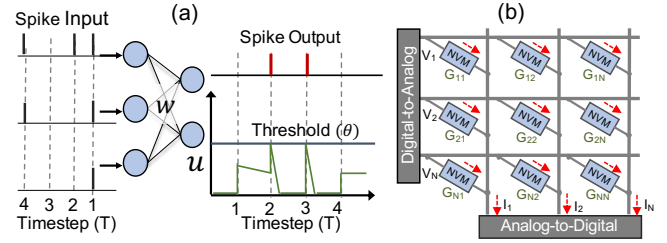


Fig. 3: (a) Pictorial representation of an SNN. (b) Pictorial representation of an $N \times N$ crossbar.

voltages V_i to each row of the crossbar by the DACs, while weights are programmed as NVM device conductances (G_{ij}) at the cross-points (we use RRAM as NVM devices in this work), as shown in Fig. 3(b).

To emulate dot-product operations in an ideal $N \times N$ crossbar during inference, input voltages interact with device conductances, generating currents according to Ohm's Law. Based on Kirchhoff's current law, the total output current sensed at each column j by the ADCs is the sum of currents flowing through all devices, expressed as $I_{j(ideal)} = \sum_{i=1}^N G_{ij} * V_i$. However, in practical applications, the analog nature of computation introduces non-idealities, such as variations in non-volatile memory (NVM) devices [18], [30]. Consequently, the net output current at each column j deviates from the ideal value $I_{j(ideal)}$, leading to significant accuracy degradation in SNNs implemented on crossbars [13], [16].

Direct Feedback Alignment (DFA): Direct Feedback Alignment (DFA) is a recent learning approach designed to address some of the key bottlenecks of traditional BP [23]. During the backward pass in DFA-based learning, as shown in Fig. 4, the feedback signals are aligned directly with the output errors e by fixed, randomized feedback matrix connections (B). This method decouples the layerwise sequential process in BP to compute gradients for each layer l ($\delta_l = e_l \cdot B_l$) simultaneously, contrary to the gradient computation $\delta_l = e_l \cdot W_l^T$ in BP. DFA, thus, enables parallel weight update of all layers by locally calculating gradients. We will see in Section IV that the compatibility of DFA with analog IMC platforms makes it a promising solution to perform online noise adaptation of deployed SNNs in real-time.

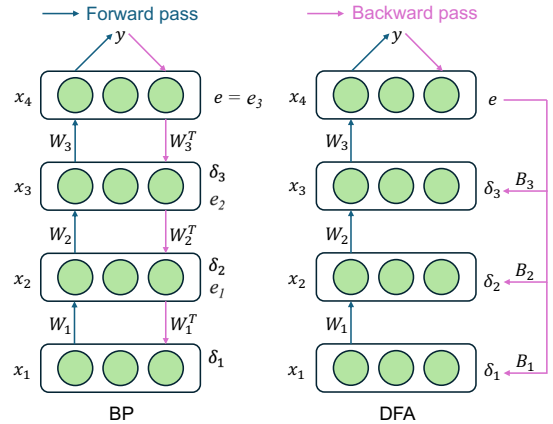


Fig. 4: Pictorial representations of BP (left) and DFA (right) learning.

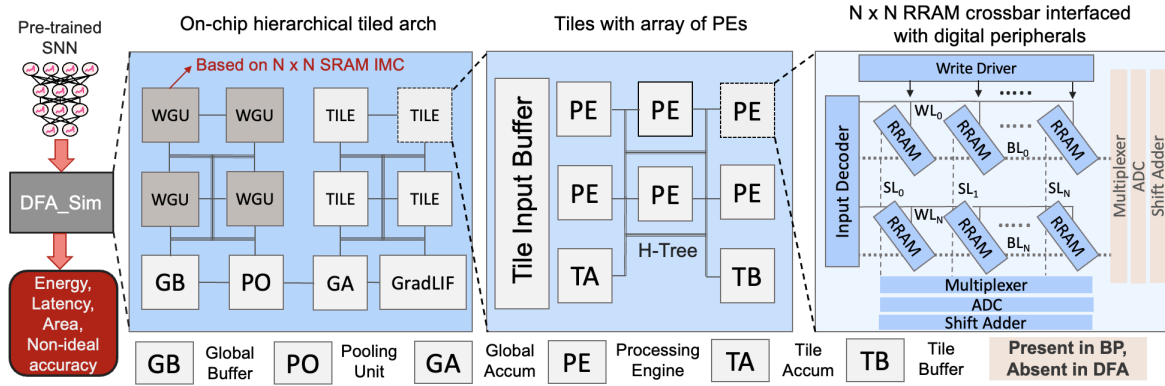


Fig. 5: Our proposed *DFA_Sim* engine. The hierarchical architecture consists of Tiles, Processing Engines (PEs) and RRAM crossbars. For DFA-based adaptation, the crossbars inside the PEs need not to be transposable. For BP-based adaptation the crossbars are transposable, thereby requiring extra peripherals. This figure is for representation purpose only; actual number of tiles, PEs and crossbars may differ.

III. *DFA_Sim*: HARDWARE EVALUATION ENGINE

Architectural Details: *DFA_Sim* is a Python-based hardware evaluation engine to benchmark energy, latency & area costs of DFA-based online adaptation of SNNs on a monolithic IMC chip built upon analog RRAM crossbars. As shown in Fig. 5, it deploys SNN models on a hierarchical, weight-stationary tiled architecture, similar to SpikeSim [17]. *DFA_Sim* features an array of interconnected tiles with global buffers, accumulators, LIF activation units, and pooling units implemented digitally. The global LIF activation unit (GradLIF), based on [31], supports LIF operations in the forward pass and gradient calculations in the backward pass. Each tile contains 4 Processing Engines (PEs), input/output buffers, and accumulation modules for partial sums. Each PE includes 4 analog 256×256 IMC crossbars using 4-bit RRAM devices [25] that perform dot-product operations, along with peripheral circuits such as input decoders, ADCs, write drivers, shift adders, etc. The PEs compute dot-products $x_l \cdot W_l$ in the forward pass and $\delta_l = e \cdot B_l$ during the backward pass (see Fig. 4) for a given SNN layer l . Weight gradients are calculated using dot-products $\delta_l \cdot x_l$ in specialized digital SRAM-based Weight Gradient Units (WGUs) [21]. Global H-trees connect tiles and the global buffer, while local H-trees manage communication within each tile and PE.

Differences between Hardware for DFA and BP: BP computes gradients $\delta_l = e_l \cdot W_l^T$ layer-by-layer (see Fig. 4), requiring transposable crossbars in PEs to handle both $x_l \cdot W_l$ in the forward pass and $e_l \cdot W_l^T$ in the backward pass. This is achieved by duplicating peripheral circuits on the row-side of the crossbars [21], [25]. In contrast, DFA removes the need for transposable crossbars, reducing the significant area overhead of peripheral circuits. However, DFA requires additional RRAM crossbars for feedback error signal computation using random B matrices. Section IV shows that the area savings from eliminating transposable crossbars outweigh the extra cost of the feedback crossbars. Another interesting facet of using RRAM crossbars is that the intrinsic stochasticity of RRAM devices can be exploited to generate and store the random B matrices [32], [33].

Mapping SNNs: For SNN weight mapping, we adopt the standard approach proposed in SpikeSim [17], assuming that no two layers of an SNN can be mapped onto the PEs within

a single tile. To enable DFA, we allocate an additional tile to store random B matrices in the RRAM crossbars. Given that this work focuses on tasks like Human Activity Recognition (HAR) that are executed on highly resource-constrained hardware, simpler SNN architectures such as multi-layer perceptrons (MLPs) are preferred (see Table I) [6]. Due to the smaller scale of the SNN architectures and the smaller size of the B matrices in DFA compared to W^T in BP, all B matrices can easily fit within a single tile (comprising 16 RRAM crossbars of size 256×256) and we consider duplication of B matrices in the crossbars to accelerate batch-training.

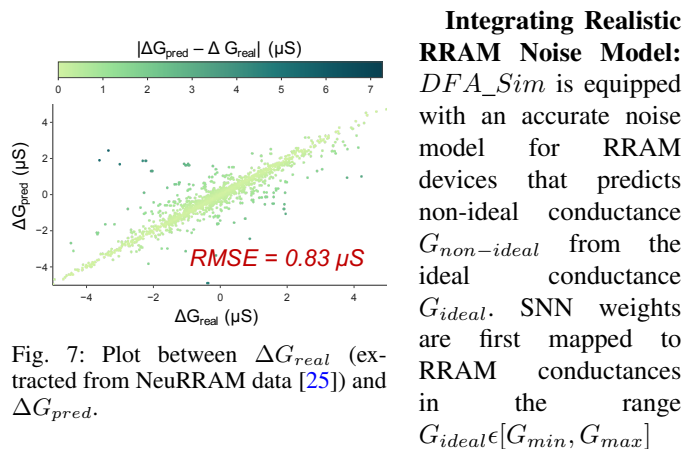


Fig. 7: Plot between ΔG_{real} (extracted from NeuRRAM data [25]) and ΔG_{pred} .

Integrating Realistic RRAM Noise Model: *DFA_Sim* is equipped with an accurate noise model for RRAM devices that predicts non-ideal conductance $G_{non-ideal}$ from the ideal conductance G_{ideal} . SNN weights are first mapped to RRAM conductances in the range $G_{ideal} \in [G_{min}, G_{max}]$

with 4-bit precision. However, when dot-product operations are carried out in the crossbars, the conductances suffer from non-idealities stemming from the RRAM device variations. We use Gaussian Process Regression (GPR) to train our RRAM noise prediction model with experimental data acquired from a real IMC chip called NeuRRAM [25] and use it to predict the noise $\Delta G = G_{non-ideal} - G_{ideal}$ injected into the programmed RRAM conductances. Before noise-modelling with GPR using the GPyTorch package, data acquired from the NeuRRAM chip was cleaned to select conductances in the range of $G_{min} = 1 \mu S$ to $G_{max} = 10 \mu S$. Thereafter, the raw data from the chip was randomly divided into training (80%, 6920 samples) and testing (20%, 1730 samples) datasets to train the noise prediction model for 100 epochs. Fig. 7 shows the fitting results with the testing dataset. We find good agreement between the ground-truth ΔG_{real} and the predicted ΔG_{pred} with an $RMSE = 0.83 \mu S$.

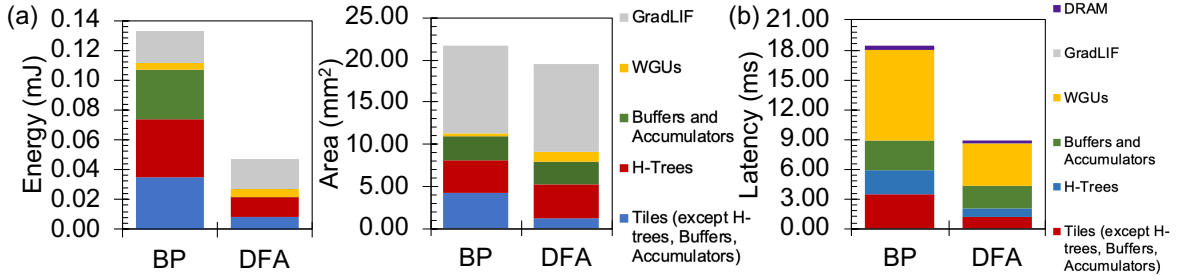


Fig. 6: Plots showing component-wise breakdown of— (a) energy per epoch (left) and area (right) for online adaptation of SNN using HHAR dataset. (b) latency per epoch (left) for online adaptation of SNN using HHAR dataset.

TABLE I: Table comparing the performance of online adaptation of SNNs using DFA and BP methods using the *DFA_Sim* engine in terms of post-adaptation non-ideal test accuracy as well as energy, latency and area for online adaptation. The best results are **highlighted**.

Timesteps (T)	SNN MLP Architecture	Task (Dataset)	Pre-trained FP32 Accuracy (%)	Pre-adaptation Non-ideal HW Accuracy (%)	Non-ideal HW Accuracy (%)		Energy (mJ)		Latency (ms)		Area (mm ²)	
					BP	DFA	BP	DFA	BP	DFA	BP	DFA
5	784-512-256-128-64-10	Fashion MNIST	88.55	61.92	83.55	85.12	0.0181	0.0072	1.9	0.947	23.1	20.1
128	9-128-64-32-6	UCI-HAR	89.68	57.22	84.93	85.61	0.0979	0.0316	15.7	8.24	21.7	19.5
100	6-256-128-64-6	HHAR	90.77	39.6	75.0	82.55	0.132	0.0474	18.1	8.67	21.7	19.5

TABLE II: *DFA_Sim* Hardware Parameters

Parameters	Data
Technology	32 nm CMOS
Operating Frequency	1 GHz
Global/Tile/PE buffer	16 KB/4 KB/1 KB
PEs per Tile, Crossbars per PE	4, 4
Crossbar size	256×256
RRAM Device Precision	4 bits
$[G_{min}, G_{max}]$	$[1\mu S, 10\mu S]$
Spike-decoder Precision	1 bit
ADC Precision	4 bits

IV. RESULTS AND DISCUSSION

Experimental Setup: We conducted experiments using BPTT-trained SNN MLPs on two human activity recognition (HAR) tasks (UCI-HAR [34] and HHAR [26]), and one image classification task (Fashion MNIST [35]), as summarized in Table I. UCI-HAR includes data from 30 subjects performing six activities (walking, walking upstairs, walking downstairs, sitting, standing, and lying) using accelerometer and gyroscope sensors from a Samsung Galaxy SII (50 Hz sampling rate). HHAR involves data from 9 subjects performing six daily activities (biking, sitting, standing, walking, stair up, and stair down) using accelerometers from 8 smartphones and 4 smartwatches (sampling rates between 50 and 200 Hz). Fashion MNIST consists of 28×28 grayscale images from 10 classes. The pre-trained SNNs were adapted online on non-ideal RRAM crossbars for 25 epochs. We used the *DFA_Sim* engine to estimate energy, latency, area and inference accuracy for DFA-based online adaptation and compared it with BP-based adaptation. Energy and latency were calculated per epoch, with a fixed training batch size of 50. Hardware details for *DFA_Sim* are listed in Table II.

From Fig. 6(a), we observe that DFA-based online adaptation for the HHAR task results in a 64.1% reduction in training energy, primarily due to lower tile-level computation and H-tree data communication costs. Note that both BP and DFA incur a constant DRAM access energy cost (17.7 mJ for the HHAR task), which is not shown in Fig. 6(a) or Table I. Additionally, DFA reduces the overall area by

10.1% compared to BP, largely because of the elimination of transposable crossbars and their associated peripherals. While DFA requires an extra tile for the $\delta_i = e \cdot B_i$ operations and a larger WGU area to handle simultaneous weight updates, the 13.4% area saved by removing transposable crossbars offsets the 3.29% increase in WGU area. Fig. 6(b) also demonstrates that DFA achieves a $2.1 \times$ overall speedup by processing all SNN layers concurrently, primarily by reducing latency at the tile, WGU, and data communication levels.

Table I presents overall results to underscore the efficacy of DFA-based online adaptation of SNNs in real-time. While naively deploying SNNs on the IMC platform significantly reduces their performance ($\sim 27 - 51\%$ loss in accuracy), online adaptation with DFA can restore their performance by reducing the accuracy losses to $\sim 3 - 8\%$, compared to the FP32 software baseline. In fact, DFA leads to better performance ($\sim 1 - 8\%$ higher non-ideal accuracy) than traditional BP-based online adaptation. This is because the layer-sequential gradient propagation in BP results in error accumulation due to non-idealities affecting the SNN weights. However, as DFA decouples gradient computations at a given SNN layer from its predecessors, error accumulation is eliminated. Furthermore, DFA achieves $\sim 60 - 68\%$ lower energy at $\sim 10 - 13\%$ lower area and $\sim 2 \times$ lower latency than BP.

V. CONCLUSION

To the best of our knowledge, this work for the first time proposes DFA as a low-cost and efficient method for online adaptation of pre-trained SNNs on resource-constrained and non-ideal edge devices. Our in-house *DFA_Sim* engine highlights the significant energy, area, and latency benefits of DFA over traditional BP for real-time learning on an RRAM-based IMC platform. Furthermore, with a realistic RRAM noise prediction model integrated with *DFA_Sim*, we show SNNs adapted using DFA to achieve better non-ideal accuracy compared to BP. These findings underscore the potential of DFA-based online adaptation for advancing low power, spike-based analytics in wearable and edge computing applications.

REFERENCES

- [1] S. Tanzarella *et al.*, “Neuromorphic decoding of spinal motor neuron behaviour during natural hand movements for a new generation of wearable neural interfaces,” *IEEE Transactions on Neural Systems and Rehabilitation Engineering*, 2023.
- [2] S. Bian *et al.*, “Evaluating spiking neural network on neuromorphic platform for human activity recognition,” in *Proceedings of the 2023 ACM International Symposium on Wearable Computers*, 2023.
- [3] “Andante,” <https://www.andante-ai.eu/>.
- [4] E. Covi, *et al.*, “Adaptive extreme edge computing for wearable devices,” *Frontiers in Neuroscience*, 2021.
- [5] S. B. Furber *et al.*, “The spinnaker project,” *Proceedings of the IEEE*, 2014.
- [6] Y. Li *et al.*, “Efficient human activity recognition with spatio-temporal spiking neural networks,” *Frontiers in Neuroscience*, 2023.
- [7] N. P. Jouppi, *et al.*, “In-datacenter performance analysis of a tensor processing unit,” in *Proceedings of the 44th annual international symposium on computer architecture*, 2017.
- [8] E. García-Martín *et al.*, “Estimation of energy consumption in machine learning,” *Journal of Parallel and Distributed Computing*, 2019.
- [9] A. Shaaban, *et al.*, “Rt-scnn: real-time spiking convolutional neural networks for a novel hand gesture recognition using time-domain mm-wave radar data,” *International Journal of Microwave and Wireless Technologies*, 2024.
- [10] L. Feng *et al.*, “Towards neuromorphic brain-computer interfaces: Model and circuit co-design of the spiking eegnet,” *Microelectronics Journal*, 2023.
- [11] N. Verma *et al.*, “In-memory computing: Advances and prospects,” *IEEE Solid-State Circuits Magazine*, 2019.
- [12] N. R. Shanbhag *et al.*, “Comprehending in-memory computing trends via proper benchmarking,” in *2022 IEEE Custom Integrated Circuits Conference (CICC)*, 2022.
- [13] A. Moitra *et al.*, “When in-memory computing meets spiking neural networks—A perspective on device-circuit-system-and-algorithm co-design,” *Applied Physics Reviews*, 2024.
- [14] A. Mehonic *et al.*, “Brain-inspired computing needs a master plan,” *Nature*, 2022.
- [15] A. Ankit *et al.*, “Resparc: A reconfigurable and energy-efficient architecture with memristive crossbars for deep spiking neural networks,” in *Proceedings of the 54th Annual Design Automation Conference 2017*, 2017.
- [16] A. Bhattacharjee *et al.*, “Examining the robustness of spiking neural networks on non-ideal memristive crossbars,” in *Proceedings of the ACM/IEEE International Symposium on Low Power Electronics and Design*, 2022.
- [17] A. Moitra, *et al.*, “Spikesim: An end-to-end compute-in-memory hardware evaluation tool for benchmarking spiking neural networks,” *IEEE Transactions on Computer-Aided Design of Integrated Circuits and Systems*, 2023.
- [18] X. Sun *et al.*, “Impact of non-ideal characteristics of resistive synaptic devices on implementing convolutional neural networks,” *IEEE Journal on Emerging and Selected Topics in Circuits and Systems*, 2019.
- [19] B. Liu *et al.*, “Vortex: Variation-aware training for memristor x-bar,” in *Proceedings of the 52nd Annual Design Automation Conference*, 2015.
- [20] I. Chakraborty *et al.*, “Technology aware training in memristive neuromorphic systems for nonideal synaptic crossbars,” *IEEE Transactions on Emerging Topics in Computational Intelligence*, 2018.
- [21] X. Peng *et al.*, “Dnn+ neurosim v2. 0: An end-to-end benchmarking framework for compute-in-memory accelerators for on-chip training,” *IEEE Transactions on Computer-Aided Design of Integrated Circuits and Systems*, 2020.
- [22] H. Jin, *et al.*, “Rehy: A rram-based digital/analog hybrid pim architecture for accelerating cnn training,” *IEEE Transactions on Parallel and Distributed Systems*, 2021.
- [23] A. Nøkland, “Direct feedback alignment provides learning in deep neural networks,” *Advances in neural information processing systems*, 2016.
- [24] I. Hossen *et al.*, “Data-driven rram device models using kriging interpolation,” *Scientific Reports*, 2022.
- [25] W. Wan *et al.*, “A compute-in-memory chip based on resistive random-access memory,” *Nature*, 2022.
- [26] A. Stisen *et al.*, “Smart devices are different: Assessing and mitigating mobile sensing heterogeneities for activity recognition,” in *Proceedings of the 13th ACM conference on embedded networked sensor systems*, 2015.
- [27] Y. Wu *et al.*, “Spatio-temporal backpropagation for training high-performance spiking neural networks,” *Frontiers in neuroscience*, 2018.
- [28] A. Paszke *et al.*, “Automatic differentiation in pytorch,” 2017.
- [29] Y. Kim *et al.*, “Rate coding or direct coding: Which one is better for accurate, robust, and energy-efficient spiking neural networks?” in *ICASSP*, 2022.
- [30] A. Bhattacharjee *et al.*, “Neat: Nonlinearity aware training for accurate, energy-efficient, and robust implementation of neural networks on 1t-1r crossbars,” *IEEE Transactions on Computer-Aided Design of Integrated Circuits and Systems*, 2021.
- [31] R. Yin *et al.*, “Sata: Sparsity-aware training accelerator for spiking neural networks,” *IEEE Transactions on Computer-Aided Design of Integrated Circuits and Systems*, 2022.
- [32] Y. Lin *et al.*, “Bayesian neural network realization by exploiting inherent stochastic characteristics of analog rram,” in *2019 IEEE International Electron Devices Meeting (IEDM)*, 2019.
- [33] A. Malhotra *et al.*, “Exploiting oxide based resistive rram variability for bayesian neural network hardware design,” *IEEE Transactions on Nanotechnology*, 2020.
- [34] D. Anguita *et al.*, “A public domain dataset for human activity recognition using smartphones.” in *Esann*, 2013.
- [35] H. Xiao *et al.*, “Fashion-mnist: a novel image dataset for benchmarking machine learning algorithms,” *arXiv:1708.07747*, 2017.